2010

Mechanical Sensorless Maximum Power Tracking Control for Direct-Drive PMSG Wind Turbines

Xu Yang
University of Nebraska-Lincoln, xu.yang@huskers.unl.edu

Xiang Gong
University of Nebraska-Lincoln, xiang.gong@huskers.unl.edu

Wei Qiao
University of Nebraska-Lincoln, wqiao@engr.unl.edu

IEEE Energy Conversion Congress and Exposition (ECCE) 2010 Atlanta, Georgia,
USA September 12-16, 2010; Pages: 4091 - 4098, DOI: 10.1109/ECCE.2010.5617749

Mechanical Sensorless Maximum Power Tracking Control for Direct-Drive PMSG Wind Turbines

Xu Yang
Student Member, IEEE
Department of Electrical Engineering
University of Nebraska-Lincoln
Lincoln, NE 68588-0511 USA
xu.yang@huskers.unl.edu

Xiang Gong
Student Member, IEEE
Department of Electrical Engineering
University of Nebraska-Lincoln
Lincoln, NE 68588-0511 USA
xiang.gong@huskers.unl.edu

Wei Qiao
Member, IEEE
Department of Electrical Engineering
University of Nebraska-Lincoln
Lincoln, NE 68588-0511 USA
wqiao@engr.unl.edu

***Abstract* – Wind turbine generators (WTGs) are usually equipped with mechanical sensors to measure wind speed and rotor position for system control, monitoring, and protection. The use of mechanical sensors increases the cost and hardware complexity and reduces the reliability of the WTG systems. This paper proposes a mechanical sensorless maximum power tracking control for wind turbines directly driving permanent magnetic synchronous generators (PMSGs). In the proposed algorithm, the PMSG rotor position is estimated from the measured stator voltages and currents by using a sliding mode observer (SMO). The wind turbine shaft speed is estimated from the PMSG back electromotive force (EMF) using a model adaptive reference system (MRAS) observer. A back propagation artificial neural network (BPANN) is designed to generate the optimal shaft speed reference in real time by using the estimated turbine shaft speed and the measured PMSG electrical power. A control system is developed for the PMSG wind turbine to continuously track the optimal shaft speed reference to generate the maximum electrical power without using any wind speed or rotor position sensors. The validity of the proposed control algorithm is shown by simulation studies on a 3-kW PMSG wind turbine and experimental results on a practical 300-W PMSG wind turbine.**

***Index Terms*—artificial neural network, model adaptive reference system (MRAS), permanent magnet synchronous generator (PMSG), sensorless control, sliding mode observer (SMO), wind turbine.**

I. INTRODUCTION

Permanent magnet synchronous generators (PMSGs) are commonly used in small and medium-size wind turbine systems for electric power generation. Compared to the wind turbines equipped with induction generators, there are several advantages of using PMSGs. First, the PMSGs can provide highly efficient and reliable power generation, since there is no need for external excitation and no copper losses in the rotor circuit. Second, the high-power-density PMSGs are small in size, which reduces the cost and weight of the wind turbine generator (WTG) system. Moreover, the wind turbine equipped with a direct-drive PMSG removes the need of using a gearbox. According to the statistical data reported in [1], approximately 19.4% downtime of WTGs is caused by failures of gearboxes. Without gearboxes, the WTG systems need less maintenance and have a reduced downtime and a higher reliability.

Control, monitoring, and protection of WTGs usually requires the information of wind speed and generator rotor position. These can be measured by well-calibrated mechanical sensors, such as anemometers and rotor position sensors. However, the use of these mechanical sensors increases the cost and failure rate of the WTG systems. According to [3], sensor failures contribute to more than 14% of failures in WTG systems and more than 40% of failures are related to the failure of sensors and the consequent failures of the control or electrical systems. Repairing the failed components requires additional cost and leads to a significant loss in electric power production.

The problems incurred in using mechanical sensors can be solved through mechanical sensorless control. In [2] and [3], the wind speed was estimated based on power signal feedback but the generator rotor position or speed was still measured for wind speed estimation and WTG control. The control systems in [4]-[6] used a hill-climbing search algorithm to track the maximum power point of the wind turbine. This method does not need the information of wind speed. However, since the wind speed changes from time to time and it takes time for this method to locate the maximum power point, the WTGs may always operate at nonoptimal conditions during operation. In [7], the wind speed was predicted for system control from an autoregressive statistical model by using historical data. Most of these works still used generator rotor position/speed measurements.

In existing WTG control systems, rotor position sensors are used not only to get the shaft speed information but also to control the frequency of the power electronic converters. The previous research on rotor position sensorless control has been focused in the area of permanent magnet (PM) motor drives. For example, in [8] a sliding mode observer was developed for rotor position sensorless control of PM motors without saliency. Reference [9] used the output voltage of the *d*-axis current regulator of the drive system to estimate the rotor position.

This paper extends the work in [2] by proposing a novel

This work was supported by the U.S. National Science Foundation under grant ECCS-0901218 and CAREER Award ECCS-0954938.

mechanical sensorless maximum power tracking control for direct-drive PMSG wind turbines. First, a sliding mode observer is designed to estimate the rotor position of the PMSG. The turbine shaft speed is then determined from a model reference adaptive system (MRAS) speed observer. Based on the measured electrical power and estimated rotor speed of the PMSG, the optimal turbine shaft speed reference is generated in real time by a BPANN. Finally, a sensorless control is developed for the PMSG wind turbine to continuously track the optimal shaft speed reference to generate the maximum electrical power without the need for any wind speed or rotor position sensors.

II. Direct-Drive PMSG Wind Turbine System

The configuration of a PMSG wind turbine is shown in Fig. 1, where the wind turbine is connected to the PMSG directly. The electrical power generated by the PMSG is transmitted to a power grid and/or supplied to a load via a variable frequency converter, which consists of a machine side converter (MSC) and a grid side converter (GSC).

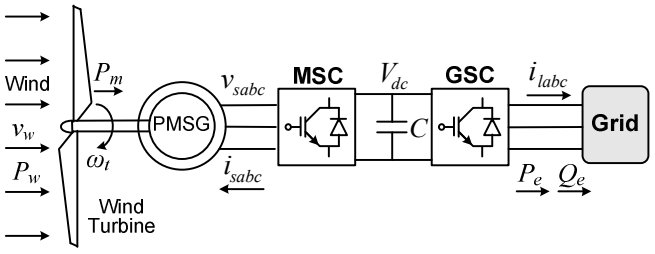

Fig. 1. Configuration of a direct-drive PMSG wind turbine.

A. Wind Turbine Aerodynamic Model

The mechanical power that a wind turbine extracts from the wind is given by:

$$P_m = \frac{1}{2}\rho A_r v_w^3 C_p(\lambda) = f(v_w, \omega_t) \tag{1}$$

where ρ is the air density; A_r is the area swept by the blades; v_w is the wind speed; C_p is the turbine power coefficient; ω_t is the turbine shaft speed. λ is the tip speed ratio, which is defined by:

$$\lambda = \frac{\omega_t R}{v_w} \tag{2}$$

where R is the radius of the blades. In this paper, C_P is given by [10]:

$$C_p = \frac{1}{2}(\lambda - 5.6)\exp(-0.17\lambda) \tag{3}$$

B. Modeling of the PMSG

The dynamic equations of a three-phase PMSG without saliency can be written in a synchronously rotating dq reference frame as:

$$v_{sq} = R_s i_{sq} + \frac{d\psi_q}{dt} + \omega_r \psi_d \tag{4}$$

$$v_{sd} = R_s i_{sd} + \frac{d\psi_d}{dt} - \omega_r \psi_q \tag{5}$$

where v_{sq} and v_{sd} are the q-axis and d-axis stator terminal voltages, respectively; i_{sq} and i_{sd} are the q-axis and d-axis stator currents, respectively; R_s is the resistance of the stator windings; ω_r (= $p\omega_t$) is the electrical angular velocity of the rotor and p is the number of pole pairs of the PMSG; and ψ_q and ψ_d are the q-axis and d-axis flux linkages of the PMSG, respectively, given by:

$$\psi_q = L_q i_{sq} \tag{6}$$

$$\psi_d = L_d i_{sd} + \psi_m \tag{7}$$

where ψ_m is the flux linkage generated by the permanent magnet. The electromagnetic torque can be calculated by

$$T_e = \frac{3}{2}\frac{p}{2}(\psi_m i_{sq} + (L_d - L_q) i_{sd} i_{sq}) \tag{8}$$

For nonsalient PMSG,

$$T_e = \frac{3}{2}\frac{p}{2}\psi_m i_{sq} \tag{9}$$

where L_q and L_d are the q-axis and d-axis inductances of the PMSG, respectively. The output electrical power can be calculated by:

$$P_e = \frac{3}{2}(v_{sd} i_{sd} + v_{sq} i_{sq}) \tag{10}$$

C. Modeling of the Shaft System

As the wind turbine is connected to the PMSG directly, the shaft system of the WTG can be represented by a one-mass model. The motion equation is then given by:

$$J\frac{d\omega_t}{dt} = \frac{P_m}{\omega_t} - \frac{P_e}{\omega_t} - D\omega_t \tag{11}$$

where J is the total inertia constant of the WTG and D is the damping coefficient.

III. Real-Time Optimal Shaft Speed Reference Determination

In a WTG system, the conversion from wind energy to generator electrical power can be illustrated by the nonlinear process in Fig.2. If the PMSG electrical power P_e and the turbine shaft speed ω_t are known, the wind speed v_w can be estimated from the inverse mapping of the WTG process in Fig.2. In addition, the relationship between the wind speed and the optimal shaft speed is given by:

$$\omega_{t,opt} = \frac{\lambda_{opt} v_w}{R} \tag{12}$$

where λ_{opt} is the optimal tip speed ratio. For the wind turbine model used in this paper, the value of λ_{opt} is 11.55. Combining (12) and the WTG process in Fig. 2 indicates that the optimal shaft speed reference can be determined directly from the PMSG electrical power P_e and the turbine shaft speed ω_t, as shown in Fig. 2.

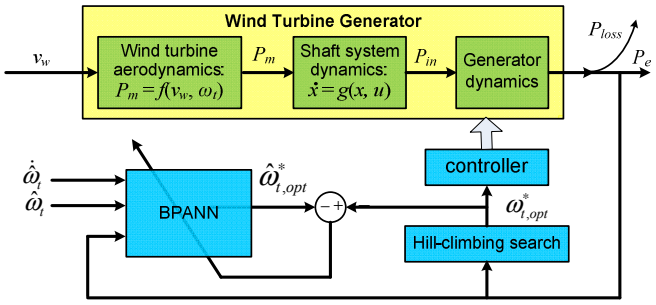

Fig. 2. BPANN-based optimal shaft speed reference determination.

In this paper, a three-layer BPANN as shown in Fig. 3 is designed to provide a nonlinear mapping from P_e, $\hat{\omega}_t$, and $\dot{\hat{\omega}}_t$ to $\omega^*_{t,opt}$, where $\hat{\omega}_t$, $\dot{\hat{\omega}}_t$, and $\hat{\omega}^*_{t,opt}$ are the estimated turbine shaft speed, the derivative of $\hat{\omega}_t$, and the estimated optimal shaft speed reference, respectively. The overall input-output mapping of the BPANN is:

$$\omega^*_{t,opt} = b + \sum_{j=1}^{h} v_j \,\text{tansig}\left(w_{1j} P_e + w_{2j}\hat{\omega}_t + w_{3j}\dot{\hat{\omega}}_t + b_j\right) \quad (13)$$

where h is the number of neurons in the hidden layer; w_{1j}, w_{2j}, and w_{3j} are the weights between the input and hidden layers; v_j is the weight between the j^{th} neuron in the hidden layer and the output; b_j and b are the bias terms of the hidden and output layers, respectively; 'tansig' is the hyperbolic tangent sigmoid transfer function, defined by:

$$\tan\text{sig}(x) = \frac{2}{1+e^{-2x}} - 1 \quad (14)$$

The parameters of the BPANN, including the weights, bias terms, and the number of neurons in the hidden layer, are determined online through a training process, as shown in Fig. 2. At each training time step, the optimal shaft speed reference $\omega^*_{t,opt}$ is generated by a hill-climbing search algorithm [4], which does not need the information of wind speed. Fig. 4 shows the principle of the hill-climbing search algorithm. In this method, the shaft speed ω_t is continuously adjusted by a constant increment/decrement of $d\omega_t$ in each search step. As a result, the output electric power P_e changes by dP_e. If $dP_e/d\omega_t > 0$, ω_t keeps increasing; otherwise, if $dP_e/d\omega_t < 0$, ω_t keeps decreasing until the maximum power point is located. The corresponding shaft speed is the optimal value $\omega^*_{t,opt}$. If the wind speed varies slowly and the time interval of the search step is sufficiently small, the shaft speed will be always around the optimal value. $\omega^*_{t,opt}$ is then compared with the estimated optimal shaft speed reference $\hat{\omega}^*_{t,opt}$ from the BPANN; and the error between them is used to adjust the parameters of the BPANN through a back-propagation algorithm [11]. The BPANN is trained until an acceptable performance is achieved. The parameters of the BPANN are then fixed operation for real-time determination of the optimal shaft speed reference.

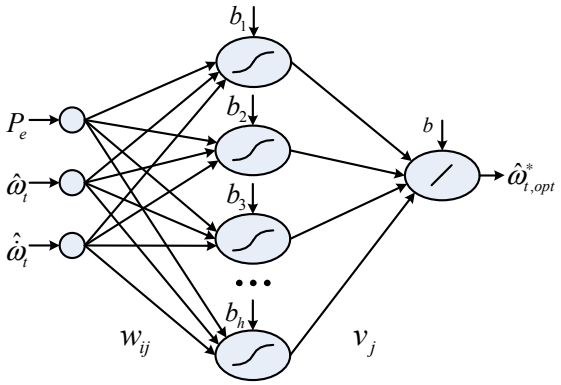

Fig. 3. Configuration of the BPANN.

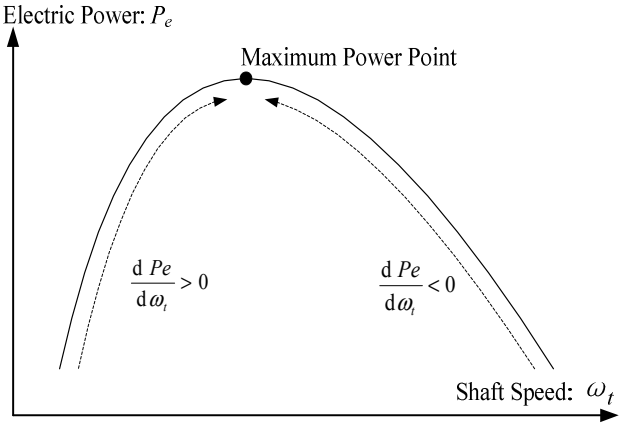

Fig. 4. The principle of the hill-climbing search algorithm.

IV. Real-Time PMSG Rotor Position and Turbine Shaft Speed Estimation

The information of the PMSG rotor position θ_r and the turbine shaft speed ω_t is needed for wind speed estimation and system control. In this paper, a sliding mode observer is designed to estimate the rotor position based on the work in [8], [14].

A. Rotor Position Estimation

The dynamic equations of a nonsalient PMSG in the stationary reference frame can be expressed as [8]:

$$\dot{i}_{\alpha\beta} = A \cdot i_{\alpha\beta} + B \cdot (v_{\alpha\beta} - e_{\alpha\beta}) \quad (15)$$

where $v_{\alpha\beta}$, $i_{\alpha\beta}$, and $e_{\alpha\beta}$ are the stator voltages and currents and the back EMF in the stationary reference frame; and

$$A = \begin{bmatrix} \frac{-R_s}{L_s} & 0 \\ 0 & \frac{-R_s}{L_s} \end{bmatrix} \qquad B = \begin{bmatrix} \frac{1}{L_s} & 0 \\ 0 & \frac{1}{L_s} \end{bmatrix}$$

$$i_{\alpha\beta} = \begin{bmatrix} i_\alpha & i_\beta \end{bmatrix}^T \qquad v_{\alpha\beta} = \begin{bmatrix} v_\alpha & v_\beta \end{bmatrix}^T$$

$$e_{\alpha\beta} = \begin{bmatrix} e_\alpha \\ e_\beta \end{bmatrix} = K_e \cdot \omega_r \cdot \begin{bmatrix} -\sin(\theta_r) \\ \cos(\theta_r) \end{bmatrix}$$

where L_s is the stator inductance and K_e is a back EMF constant. Then the sliding mode observer is designed as follows [14].

$$\dot{\hat{i}}_{\alpha\beta} = A \cdot \hat{i}_{\alpha\beta} + B \cdot v_{\alpha\beta} + K_{sw} \operatorname{sgn}(\hat{i}_{\alpha\beta} - i_{\alpha\beta}) \tag{16}$$

where $\hat{i}_{\alpha\beta}$ is the estimated value of $i_{\alpha\beta}$ and K_{sw} is the switching gain of the observer.

Fig. 5 shows the block diagram of the observer, where k is the switching gain of the discontinuous control signal $Z_{\alpha\beta}$; $\hat{e}_{\alpha\beta}$ is the estimated value of the back EMF; and $\hat{\theta}_r$ is the estimated rotor position. To ensure the convergence of the sliding mode observer, K_{sw} should be selected such that $\varepsilon_{is} \cdot \varepsilon_{is}^T < 0$, where $\varepsilon_{is} = \hat{i}_{\alpha\beta} - i_{\alpha\beta}$ [14].

The estimated back EMF is obtained from the switching signal $Z_{\alpha\beta}$ by using a low-pass filter.

$$\begin{cases} \hat{e}_\alpha = \dfrac{\omega_{cutoff}}{s + \omega_{cutoff}} Z_\alpha \\ \hat{e}_\beta = \dfrac{\omega_{cutoff}}{s + \omega_{cutoff}} Z_\beta \end{cases} \tag{17}$$

The rotor position is then obtained as:

$$\hat{\theta}_r = -\tan^{-1}\left(\frac{\hat{e}_\alpha}{\hat{e}_\beta}\right) \tag{18}$$

The low-pass filter is designed to have a variable cutoff frequency according to the rotor speed [14]. The phase angle delay caused by the filter is

$$\Delta\theta_r = \tan^{-1}\left(\frac{\omega}{\omega_{cutoff}}\right) \tag{19}$$

The delayed angle is compensated for the estimation of the rotor angle position.

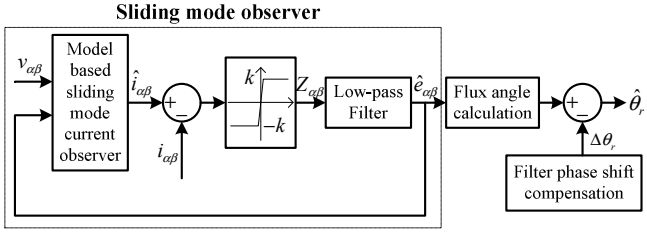

Fig. 5. Block diagram of the sliding mode observer.

B. PMSG Rotor/Turbine Shaft Speed Estimation

The turbine shaft speed can be simply calculated from the derivative of the PMSG rotor angle. However, in this paper the turbine shaft speed is obtained from a back EMF-based MRAS observer [15]. This method has a better performance than the rotor angle derivative-based method for turbine shaft speed estimation. According to (15), if the PMSG rotor speed changes slowly, i.e., $\dot{\omega}_r \approx 0$, the reference model of the induced back EMF is:

$$\dot{e}_\alpha = -\omega_r \cdot e_\beta \quad \text{and} \quad \dot{e}_\beta = \omega_r \cdot e_\alpha \tag{20}$$

The adjustable model is designed as [16]

$$\begin{cases} \dot{\tilde{e}}_\alpha = -\tilde{\omega}_r \cdot \hat{e}_\beta - L \cdot (\tilde{e}_\alpha - \hat{e}_\alpha) \\ \dot{\tilde{e}}_\beta = \tilde{\omega}_r \cdot \hat{e}_\alpha - L \cdot (\tilde{e}_\beta - \hat{e}_\beta) \end{cases} \tag{21}$$

where L is a constant gain; $\hat{e}_\alpha$ and $\hat{e}_\beta$ are the back EMF components obtained from the sliding mode observer; $\tilde{e}_\alpha$ and $\tilde{e}_\beta$ are the estimated values of $\hat{e}_\alpha$ and $\hat{e}_\beta$, respectively, from the MRAS observer. The adaptation mechanism for the MRAS system is derived by using the hyper stability criteria as follows [17].

$$\hat{\omega}_r = (k_p + \frac{k_i}{s})[(\tilde{e}_\alpha - \hat{e}_\alpha) \cdot \tilde{e}_\beta - (\tilde{e}_\beta - \hat{e}_\beta) \cdot \tilde{e}_\alpha] \tag{22}$$

Fig. 6 illustrates the block diagram of the MRAS rotor speed observer. The back EMFs are normalized as follows:

$$e = \frac{1}{\sqrt{e_\alpha^{\,2} + e_\beta^{\,2}}} \begin{bmatrix} e_\alpha \\ e_\beta \end{bmatrix} \tag{23}$$

where e stands for $\hat{e}$ or $\tilde{e}$. In Fig. 6, $J = \begin{bmatrix} 0 & -1 \\ 1 & 0 \end{bmatrix}$ and ε is the estimation error of the normalized back EMF. The turbine shaft speed ω_t can be obtained from $\hat{\omega}_r$ directly.

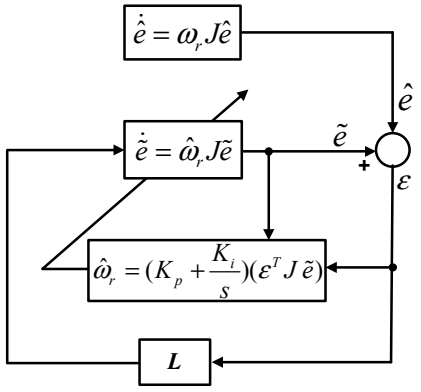

Fig. 6. Back EMF-based MRAS PMSG rotor speed observer.

V. SENSORLESS CONTROL FOR PMSG WIND TURBINES

In the proposed estimation algorithms, both the PMSG rotor position and turbine shaft speed are estimated from the measured stator voltages v_{sabc} and currents i_{sabc}. The estimated rotor position $\hat{\theta}_r$ is used in the MSC control system to correctly transform the three-phase stator voltages and currents into the rotor reference frame. The estimated rotor position and turbine shaft speed are integrated into the control system, leading to a sensorless control for the PMSG wind turbine, as shown in Fig. 7. The overall control system consists of two parts: control of the MSC and control of the

GSC. The MSC control tracks the maximum power point of the wind turbine. The objective of the GSC is to transfer the active power generated by the PMSG to the grid and/or load by controlling a constant DC-link voltage. The GSC can also be arranged to control the reactive power, voltage, or power factor at the AC terminals.

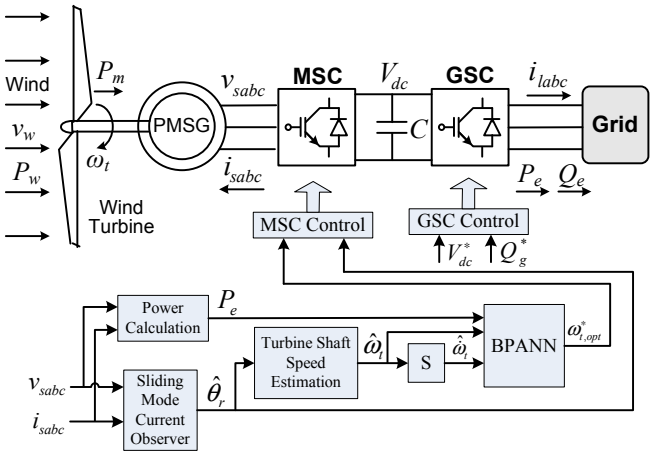

Fig. 7. The proposed sensorless control for the PMSG wind turbine.

A. Design of the MSC Controllers

The overall MSC control scheme consists of two loops, as shown in Fig. 8. The inner-loop PI controllers regulate the *d*-axis and *q*-axis stator currents of the PMSG according to the models of the PMSG described by (4) and (5) [19]. The outer-loop speed control tracks the optimal shaft speed reference to generate the maximum power from the WTG. The maximum torque per ampere is obtained by setting $i_{sd} = 0$ [9].

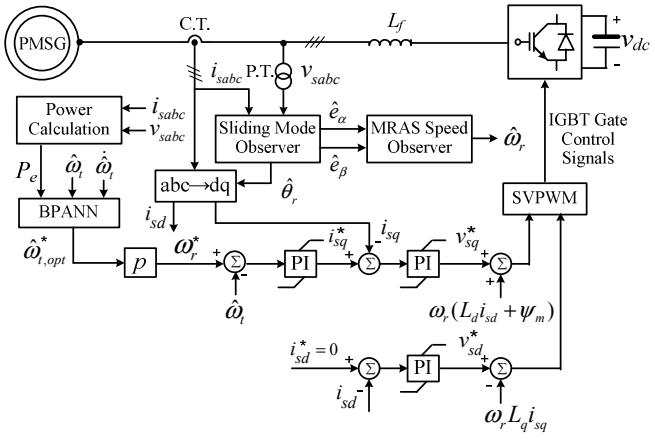

Fig. 8. Overall control scheme of the MSC.

B. Design of the GSC Controllers

The overall GSC control scheme also consists of two control loops, as shown in Fig. 9. The inner-loop PI controllers regulate the *d*-axis and *q*-axis currents i_{gd} and i_{gq} at the AC terminals of the GSC. The outer-loop controllers regulate the dc-link voltage as well as the reactive power at the AC terminals of the GSC at the desired values [18].

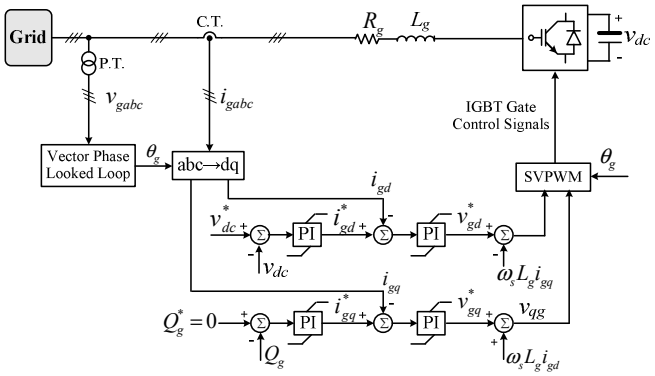

Fig. 9. Overall control scheme of the GSC.

C. Stability Analysis of the MSC Controllers

The *q*-axis current control loop of the MSC is shown in Fig. 10. Define K_p and K_i as the proportional and integral gains of the PI controller in the current loop, respectively, it can be obtained from Fig. 10 that

$$\frac{i_{sq}}{\hat{\varepsilon}_{wr}} = \frac{s}{L_s s^2 + (R_s + K_p)s + K_i} \tag{24}$$

$$\frac{i_{sq}}{i_{sq}^*} = \frac{K_p s + K_i}{L_s s^2 + (R_s + K_p)s + K_i} \tag{25}$$

where $\hat{\varepsilon}_{wr}$ is the error of the estimated turbine shaft speed. If the PI controller is well designed, the current loop is stable and the errors of the observer do not generate steady-sate errors in the current loop.

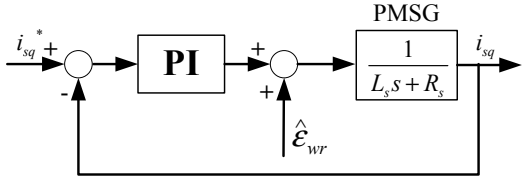

Fig. 10. MSC *q*-axis current control loop.

The PMSG rotor speed controller is shown in Fig. 11, where T_e is the electromagnetic torque; T_L is the load torque; T_o is the time constant of the speed observer; and $\hat{\varepsilon}_{wr}$ is the estimation error of the speed observer. The MSC is assumed to be ideal, and therefore, is represented by a constant 1. In a well designed observer, T_o is much smaller than other time constants. Therefore, T_o is set to 0 in the stability analysis.

Define K_{pw} and K_{iw} as the proportional and integral gains, respectively, of the PI controller in the speed control loop in Fig. 11, the transfer function between $\hat{\varepsilon}_{wr}$ and ω_r is then given by:

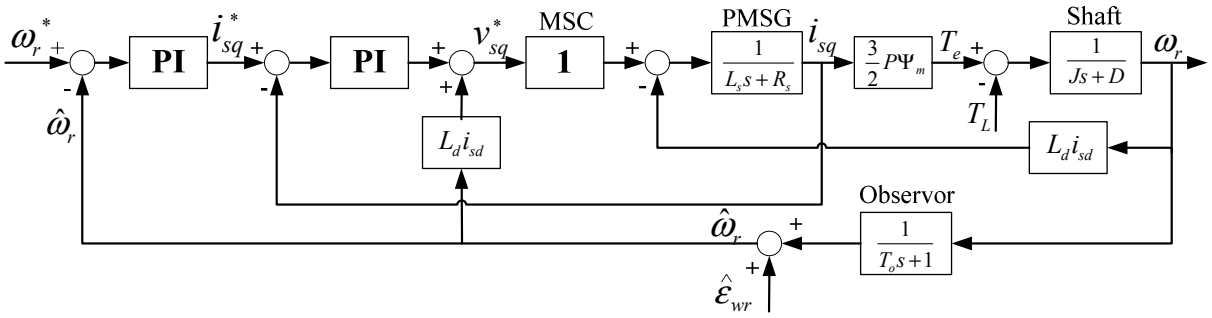

Fig. 11. The PMSG rotor speed controller.

$$\frac{\omega_r}{\hat{\varepsilon}_{wr}} = \frac{1-(K_p+\frac{K_i}{s})(K_{pw}+\frac{K_{iw}}{s})}{(K_p+\frac{K_i}{s})(K_{pw}+\frac{K_{iw}}{s})+(L_s s+R_s+K_p+\frac{K_i}{s})\frac{2(Js+D)}{3p\Psi_m}} \quad (26)$$

K_p, K_i, K_{pw}, and K_{iw} should be chosen such that the poles of the right hand side of (26) are all smaller than zero. Therefore, the system is stable with the observer error of $\hat{\varepsilon}_{wr}$.

VI. Simulation Results

Simulation studies are carried out in PSCAD to validate the proposed real-time wind speed and rotor position estimation algorithms and sensorless control for a 3-kW PMSG wind turbine. The WTG system has the following parameters. For the wind turbine: the radius of the blades is R = 2 m; the air density is ρ = 1.15kg/m^3; λ_{opt} = 11.55; the $C_p(\lambda)$ is given by (3). For the PMG: the rated power is 3 kW, R_s = 0.2499 ohms; L_d = 34.3mH; L_q = 34.3 mH; the flux linkage ψ_m = 1.0 V·s; the number of pole pairs is p = 7; and the moment of inertia is J = 1 kg·m^2.

During the simulation, the wind speed varies in the range of ±3 m/s around the mean value of 8 m/s. Figs. 12 and 13 compare the actual and estimated values of the PMSG rotor position and shaft speed. The results show that the proposed algorithm accurately estimates the PMSG rotor position and shaft speed, which are used for real-time control of the PMSG and converters.

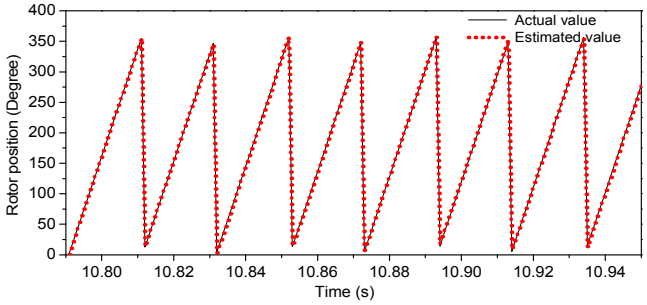

Fig. 12. PMSG rotor position estimation results.

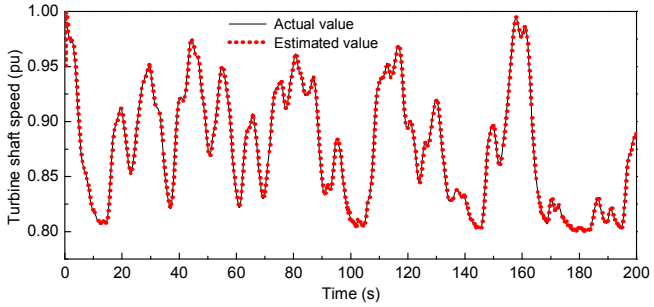

Fig. 13. Turbine shaft speed estimation results.

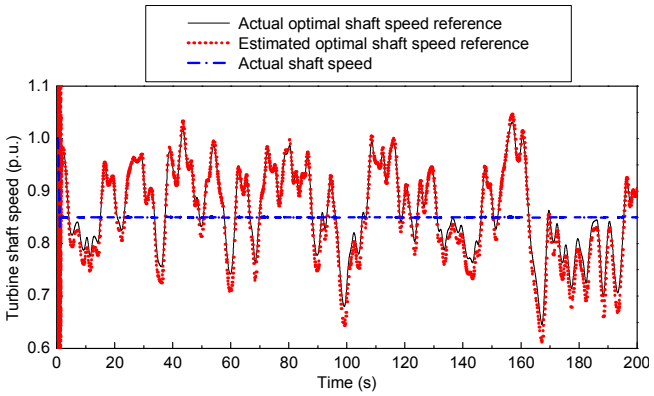

Fig. 14. Optimal shaft speed reference estimation results during constant shaft speed operation.

Figs. 14-16 compare the estimated optimal shaft speed reference generated by the BPANN with the actual optimal shaft speed reference determined by (13) using the actual wind speed for three scenarios: 1) constant shaft speed operation (Fig. 14), 2) a ramp change in shaft speed (Fig. 15), and 3) variable shaft speed operation (Fig. 16). In first two scenarios, the maximum power tracking control is not applied; while in the third scenario, the estimated optimal shaft speed reference is applied to the control the WTG to generate the maximum power. These results show that the proposed BPANN-based algorithm correctly estimates the optimal shaft speed reference for maximum power generation during various conditions. Fig. 17 shows the shaft speed tracking results in the third scenario. The turbine shaft speed is well

controlled to track the reference with good precision by using the estimated rotor position, shaft speed, and the proposed sensorless control algorithm.

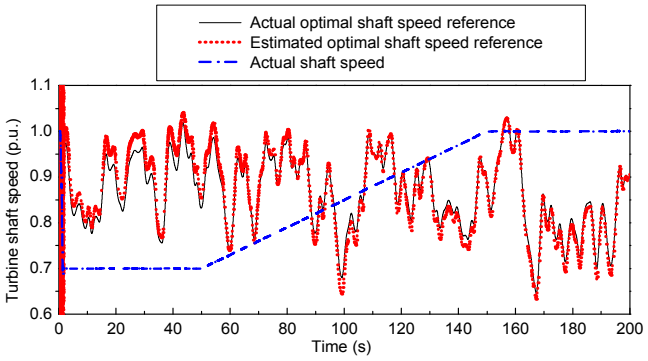

Fig. 15. Optimal shaft speed reference estimation results during a ramp change in shaft speed.

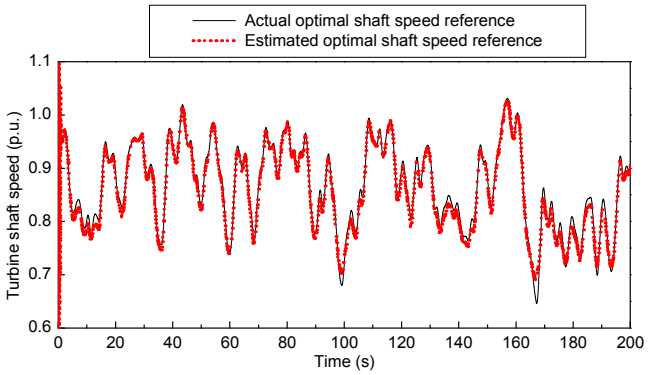

Fig. 16. Optimal shaft speed reference estimation results during variable shaft speed operation.

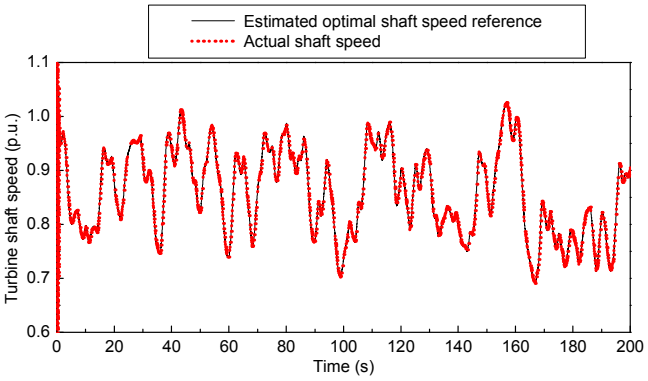

Fig. 17. Shaft speed tracking results.

VII. Experimental Results

A practical 300-W direct-drive PMSG wind turbine system has been set up to further validate the proposed PMSG rotor position and speed estimation and optimal turbine shaft speed determination algorithms. Fig. 18 illustrates the experimental setup. The PMSG is driven by an adjustable speed induction motor drive system, which emulates the dynamics of the wind turbine. An incremental encoder with 2500 pluses per revolution is used to measure the turbine shaft speed in real time. The proposed estimation algorithms are implemented in a dSPACE system.

To demonstrate the performance of the proposed speed estimation algorithms, the rotating speed of the induction motor in Fig. 18 is varied to emulate variable wind speed condition. By using the measured PMSG stator voltages and currents, the PMSG rotor speed (i.e., the turbine shaft speed) is accurately estimated by using the proposed method, as shown in Fig. 19.

The optimal turbine shaft speed reference is obtained from the BPANN in Fig. 3. By using the measured PMSG electrical power and the estimated turbine shaft speed, the optimal turbine shaft speed references are correctly determined from the proposed BPANN-based method. As shown in Fig. 20, the estimated optimal turbine shaft speed reference tracks the real optimal turbine shaft speed reference with good precision.

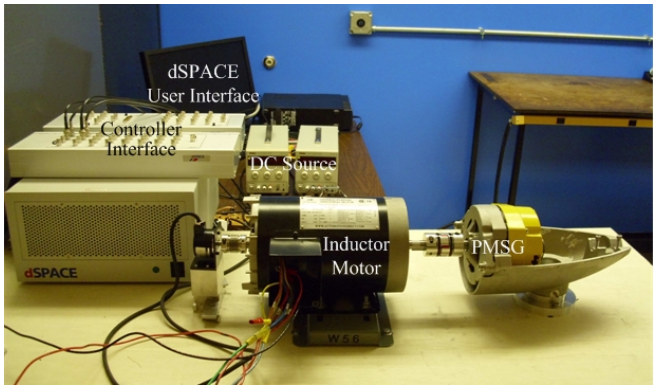

Fig. 18. Experiment setup for a 300-W PMSG wind turbine

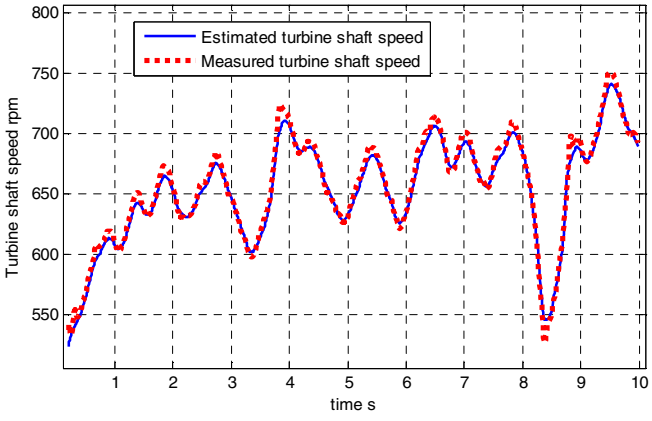

Fig. 19. Measured and estimated turbine shaft speed.

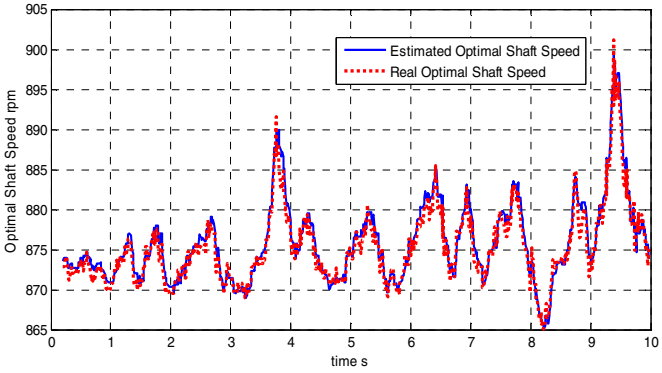

Fig. 20. Real and estimated optimal turbine shaft speed references.

VIII. CONCLUSION

This paper has proposed a mechanical sensorless control algorithm for maximum wind power generation using direct-drive PMSG wind turbines. The values of the PMSG rotor position and speed have been estimated from the measured stator voltages and currents in real time. Based on these estimated variables and the measured PMSG electrical power, the optimal turbine shaft speed reference has been determined by a BPANN and used for optimal control of the power electronic converters and the PMSG. Therefore, the commonly used mechanical sensors in WTG systems, i.e., the wind speed sensors and rotor position sensors, are not needed. The effectiveness of the proposed sensorless control has been demonstrated by simulation results of a 3-kW PMSG wind turbine. A practical 300-W PMSG wind turbine system has been set up to further validate the proposed rotor position, shaft speed, and BPANN-based optimal shaft speed reference estimation algorithms. The proposed mechanical sensorless control algorithm reduced the cost and improved the reliability of the PMSG wind turbine systems.

REFERENCES

[1] J. Ribrant and L. M. Bertling, "Survey of failures in wind power systems with focus on Swedish wind power plants during 1997-2005," *IEEE Trans. Energy Conversion*, vol. 22, no. 1, pp. 167-173, Mar. 2007.

[2] W. Qiao, W. Zhou, J. M. Aller, and R. G. Harley, "Wind speed estimation based sensorless output maximization control for a wind turbine driving a DFIG," *IEEE Trans. Power Electronics*, vol. 23, no. 3, pp. 1156-1169, May 2008.

[3] B. Boukhezzar and H. Siguerdidjane, "Nonlinear control of variable speed wind turbines without wind speed measurement," in *Proc. 44th IEEE Conference on Decision and Control*, Seville, Spain, Dec. 12-15, 2005, pp. 3456-3461.

[4] T. Tanaka and T. Toumiya, "Output control by Hill-Climbing method for a small wind power generating system," *Renewable Energy*, vol. 12, no. 4, pp. 387-400, 1997.

[5] M. G. Simoes, B. K. Bose, and R. J. Spiegel, "Fuzzy logic based intelligent control of a variable speed cage machine wind generation system," *IEEE Trans. Power Electronics*, vol. 12, no. 1, pp. 87-95, Jul./Aug. 1997.

[6] Q. Wang and L. Chang, "An intelligent maximum power extraction algorithm for inverter-based variable speed wind turbine systems," *IEEE Trans. Power Electronics*, vol. 19, no. 5, pp. 1242-1249, Sept. 2004.

[7] K. Tan and S. Islam, "Optimal control strategies in energy conversion of PMSG wind turbine system without mechanical sensors," *IEEE Trans. Energy Conversion,* vol. 19, no. 2, pp. 392-399, Jun. 2004.

[8] S. Chi and L. Xu, "Position sensorless control of PMSM based on a novel sliding mode observer over wide speed range," in *Proc. 5th International Power Electronics and Motion Control Conference,* Aug. 14-16, 2006,.

[9] J. Seok, J. Lee, and D. Lee, "Sensorless speed control of nonsalient permanent-magnet synchronous motor using rotor-position-racking PI controller," *IEEE Trans. Industrial Electronics,* vol. 53, no. 2, pp. 399-405, Apr. 2006.

[10] P. M. Anderson and A. Bose, "Stability simulation of wind turbine systems," *IEEE Trans. Power App. Syst.,* vol. PAS-102, no.12, pp. 3791-3795, Dec. 1983.

[11] N Urasaki, T Senjyu, and K Uezato, "Investigation of Influences of Various Losses on Electromagnetic Torque for Surface-Mounted Permanent Magnet Synchronous Motors," *IEEE Trans. Power Electronics,* vol. 18, no. 1, pp. 131-139, Jan. 2003.

[12] A. Grauers, "Efficiency of three wind energy generator systems," *IEEE Trans. Energy Conversion,* vol. 11, no. 3, pp. 650-657, Sept. 1996.

[13] S. J. Chapman, *Electric Machinery Fundamentals,* New York: McGraw-Hill, 2005.

[14] K. Kang, J. Kim, K. Hwang, and K. Kim, "Sensorless control of PMSM in high speed range with iterative sliding mode observer," in *Proc. 2004 IEEE Applied Power Electronic Conference and Exposition,* vol. 2, pp. 1111-1116.

[15] M. N. Marwali and A. Keyhani, "A comparative study of rotor flux based MRAS and back EMF based MRAS speed estimators for speed sensorless vector control of induction machines," in *Proc. 1997 IEEE IAS Annual Meeting*, vol. 1, pp. 160-166.

[16] C. Li and M. Elbuluk, "A sliding mode observer for sensorless control of permanent magnet synchronous motors," in *Proc. 2001 IEEE IAS Annual Meeting,* vol. 2, pp.1273-1278.

[17] F.Z. Peng and T. Fukao, "Robust speed identification for speed sensorless vector control of induction motors," *IEEE Trans. Industry Applications*, vol. 30, pp. 1234-1240, 1994.

[18] W. Qiao, "Dynamic modeling and control of doubly fed induction generators driven by wind turbines," in *Proc. 2009 IEEE PES Power Systems Conference and Exposition,* pp. 1-8.

[19] M. Chinchilla, S. Arnaltes and J. C. Burgos, "Control of Permanent-magnet generators applied to variable-speed wind-energy systems connected to the grid," *IEEE Trans. Energy Conversion*, vol.21, pp. 130-135, 2006.